

Geography-aware Optimal UAV 3D Placement for LOS Relaying: A Geometry Approach

Yuanshuai Zheng, and Junting Chen

Abstract

Many emerging technologies for the next generation wireless network prefer line-of-sight (LOS) propagation conditions to fully release their performance advantages. This paper studies 3D unmanned aerial vehicle (UAV) placement to establish LOS links for two ground terminals in deep shadow in a dense urban environment. The challenge is that the LOS region for the feasible UAV positions can be arbitrary due to the complicated structure of the environment. While most existing works rely on simplified stochastic LOS models and problem relaxations, this paper focuses on establishing theoretical guarantees for the optimal UAV placement to ensure LOS conditions for two ground users in an actual propagation environment. It is found that it suffices to search a bounded 2D area for the globally optimal 3D UAV position. Thus, this paper develops an exploration-exploitation algorithm with a linear trajectory length and achieves above 99% global optimality over several real city environments being tested in our experiments. To further enhance the search capability in an ultra-dense environment, a dynamic multi-stage algorithm is developed and theoretically shown to find an ϵ -optimal UAV position with a search length $O(1/\epsilon)$. Significant performance advantages are demonstrated in several numerical experiments for wireless communication relaying and wireless power transfer.

Index Terms

UAV, Positioning, LOS relaying, Geography-aware, Wireless power transfer

I. INTRODUCTION

The line-of-sight (LOS) propagation conditions are desired in many trending technologies for the next generation wireless networks. For example, millimeter-wave and terahertz signals have much less diffractive and reflective paths compared to sub-6GHz signals due to their small wavelengths, and hence, non-line-of-sight (NLOS) terminals usually suffer from great path loss [1, 2]. Free-space optical signals are difficult to penetrate obstacles. Wireless power transfer

(WPT) also prefers LOS conditions for energy efficiency. However, it is challenging to establish LOS conditions in a dense urban area, where high buildings and trees easily block the signals.

Low altitude unmanned aerial vehicle (UAV) provides a promising solution to establish LOS links to ground terminals in deep shadow [3, 4]. Recent works have discussed employing UAVs in many scenarios, including communication relaying, data collection, coverage extension, and WPT [5]–[9]. To mitigate the potential issue of the limited propulsion energy at the UAVs, some recent works have proposed solutions including dynamic service landing spots [10] and the applications of tethered UAVs [11]–[13].

Despite many existing works on UAV placement for wireless communications, very few solutions guarantee to establish LOS conditions for specific users in deep shadow. Most existing works tend to oversimplify the terrain environment. For example, some early works [14]–[16] studied UAV placement using a pure LOS model, assuming no blockage from the terrain. A probabilistic LOS model for urban environment was established in [17, 18], with extensions in [19, 20], and was adopted in [21]–[24] for UAV placement and trajectory planning. Since the models [21]–[24] capture the LOS conditions only in a *statistical* sense, the corresponding solutions developed in [21]–[24] cannot guarantee LOS conditions for specific users.

Some recent attempts exploit radio maps or city maps to assist UAV placement, where radio maps describe the channel quality between a ground terminal and a possible UAV position [25, 26]. Yet, it is still challenging to search for the best UAV position. The work [25] applied deep reinforcement learning (DRL) to assist the navigation of UAV, but the optimality and complexity are difficult to analyze. In [26] and [27], the authors used signal-to-interference-plus-noise ratio (SINR) map-based methods to solve the UAV 3D path planning problem, but these methods require offline city maps or radio maps, and hence, they are difficult to be applied to online search. In [28], a geometry-based approach was developed to optimize the UAV position for free-space optical relaying for two ground users, but the approach only guarantees the optimality in a 2D plane. In [29], the buildings were approximately modeled as a set of polyhedrons, and a number of constraints on the UAV positions were formulated using geometry relations; accordingly, a non-convex UAV placement problem was formed and relaxation-based algorithms were developed, although the global optimality was still unknown. In summary, the main challenge of the UAV placement problem originates from the fact that the terrain obstacles may have arbitrary locations and shapes, and therefore, the placement problems are generally non-convex with possibly arbitrarily many local optima.

In this paper, we attempt to establish some theoretical guarantees for the optimal UAV placement to ensure LOS conditions for two ground users in an almost arbitrary urban environment. The goal is to develop an efficient search strategy to explore only a small 2D local area for the best 3D UAV placement. Some prior work [30] attempted a special case of the problem, where one of the users is placed on a high tower such that there is always an LOS link between the user and the UAV. However, when both users are on the ground and are likely shadowed by buildings, the method in [30] fails to apply.

This paper exploits two universal properties for any LOS patterns from an almost arbitrary terrain structure: *upward invariance* and *colinear invariance*. Specifically, if a UAV sees a user, such an LOS condition will remain if the UAV increases its altitude or moves away from the user without changing the elevation and azimuth angles, under some additional mild conditions. Exploiting these properties, two search strategies are developed. The key theoretical results and numerical findings are summarized as follows.

- We develop a search trajectory, Algorithm 1, on the middle perpendicular plane of the two users. It is proven that the search finds the optimal solution on the middle perpendicular plane, and the search length is upper bounded by a linear function of the altitude of the initial point.
- We show that given a double-LOS initial point, it suffices to search a bounded 2D local area for the globally 3D optimal UAV position. With this analytical insight, we develop Algorithm 2 with search complexity $O(1/\epsilon)$ for the ϵ -optimal UAV position in 3D under some mild condition.
- We conduct numerical experiments using real city map data for several typical cities. It is found that both Algorithms 1 and 2 achieve over 99% optimality in a moderate dense environment. In a simulated ultra dense environment based on a street map of Guangzhou, China, Algorithm 2 can achieve over 98% of the global optimality under a reasonable search distance.

The remaining part of the paper is organized as follows. Section II introduces the system model, and formulates a geography-aware UAV position optimization problem that can be employed in multiple applications. Section III presents Algorithm 1 for the optimal solution on the middle perpendicular plane with theoretical proof of the optimality and linear complexity. In Section IV, we further propose Algorithm 2 based on the extracted geographic features of

LOS patterns, and demonstrate the performance-complexity trade-off. Section V contains our simulations accompanied by the relevant discussion and comparison, and finally, the paper is concluded in Section VI.

II. SYSTEM MODEL

A. Blockage-aware Air-to-ground Channel Model

Consider to place a UAV to establish LOS channels to two users located at \mathbf{u}_1 and \mathbf{u}_2 on the ground in an outdoor urban environment. The UAV is deployed with a minimum height H_{\min} which is set to be greater than the tallest structure in the area such that there will be no potential collision for the UAV. The users are possibly surrounded by urban structures, and thus, the wireless communication link between the UAV and the user can be blocked by buildings or trees.

For presentation convenience, define a Cartesian coordinate system with the origin O set at $(\mathbf{u}_1 + \mathbf{u}_2)/2$, and three orthonormal basis vectors \mathbf{e}_1 , \mathbf{e}_2 , and \mathbf{e}_3 where $\mathbf{e}_2 = (\mathbf{u}_2 - \mathbf{u}_1)/\|\mathbf{u}_2 - \mathbf{u}_1\|_2$ representing the direction from user 1 to user 2, \mathbf{e}_3 is the direction perpendicular to the ground pointing upward, and \mathbf{e}_1 is determined according to the right-hand rule as illustrated in Fig. 2.

Denote $\mathcal{D}_0^{(i)}$ as the set of permissible UAV positions $\mathbf{p} = (p_1, p_2, p_3)$ such that there is an LOS link between the UAV and the i th user, $i = 1, 2$, and $p_3 \geq H_{\min}$. The LOS regions $\mathcal{D}_0^{(i)}$ can be *arbitrary* except that we assume $\mathcal{D}_0^{(i)}$ have the following properties: For any $\mathbf{p} \in \mathcal{D}_0^{(i)}$,

- 1) Upward invariant: any position \mathbf{p}' perpendicularly above \mathbf{p} also belongs to $\mathcal{D}_0^{(i)}$, *i.e.*, $\mathbf{p}' \in \mathcal{D}_0^{(i)}$;
- 2) Colinear invariant: any position \mathbf{p}' that satisfies $\mathbf{p}' - \mathbf{u}_i = \rho(\mathbf{p} - \mathbf{u}_i)$ for some $\rho > 1$ also belongs to $\mathcal{D}_0^{(i)}$, *i.e.*, $\mathbf{p}' \in \mathcal{D}_0^{(i)}$.

In addition, define *double-LOS* region $\tilde{\mathcal{D}}_0 = \mathcal{D}_0^{(1)} \cap \mathcal{D}_0^{(2)}$ as the set of UAV positions where there are LOS links to both users. Since the double-LOS region is an intersection of $\mathcal{D}_0^{(i)}$, the upward invariant property automatically holds, *i.e.*, for any double-LOS position $\mathbf{p} \in \tilde{\mathcal{D}}_0$, any position \mathbf{p}' perpendicularly above \mathbf{p} is also a double-LOS position which satisfies $\mathbf{p}' \in \tilde{\mathcal{D}}_0$. Note that the colinear invariant property does not hold for $\tilde{\mathcal{D}}_0$.

To summarize, the upward invariant and colinear invariant properties imply that if a UAV sees a user at \mathbf{u}_i , such an LOS condition will remain if the UAV increases its altitude or moves away from the user without changing the elevation and azimuth angles. The widely adopted

probabilistic LOS model in the UAV literature [21]–[24] is a special case that satisfies these properties in a statistical sense.

The upward invariant and colinear invariant properties can be easily understood from the ray-tracing mechanism based on the geometry relation with the environment. The implication is that if the urban structures all have their top no wider than the base, for instance, a combination of straight pillars and cones, then the upward invariant and colinear invariant properties can be automatically satisfied. While practical city topologies may occasionally violate these properties in some local area, these properties still serve as a good approximation to the radio environment of interest.

B. Geography-aware UAV Position Optimization

The goal of this paper is to place the UAV as close to both users as possible under the double-LOS condition $\mathbf{p} \in \tilde{\mathcal{D}}_0$. Specifically, denote $f(d_i(\mathbf{p}))$ as the value function in terms of the distance $d_i(\mathbf{p}) = \|\mathbf{p} - \mathbf{u}_i\|_2$ from the UAV position \mathbf{p} to the user \mathbf{u}_i , $i \in \{1, 2\}$. The function $f(d)$ is assumed to be continuous and decreasing in d . The objective is to maximize the performance of the worse link under the double-LOS condition:

$$\begin{aligned} \mathcal{P} : \quad & \underset{\mathbf{p}}{\text{maximize}} && F(\mathbf{p}) \\ & \text{subject to} && \mathbf{p} \in \tilde{\mathcal{D}}_0 \end{aligned} \tag{1}$$

where $F(\mathbf{p}) = \min\{f(d_1(\mathbf{p})), f(d_2(\mathbf{p}))\}$.

Typical applications of the above formulation include UAV-assisted relay communications, WPT to ground devices, and video monitoring of two ground spots. In decode-and-forward relaying, for instance, one may choose $f(d) = B \log_2(1 + \gamma d^{-\alpha})$, where B is the bandwidth, γ is the effective signal-to-noise ratio (SNR), and α is the path-loss exponent in LOS (see Section V for a more specific example). For WPT or visual monitoring, the link performance function can be chosen as $f(d) = \kappa d^{-\alpha}$, where κ and α are some parameters depending on the applications.

The main challenge is due to the possibly complicated structure of the double-LOS region $\tilde{\mathcal{D}}_0$. First, $\tilde{\mathcal{D}}_0$ may appear to have an irregular pattern as shown in Fig. 1, where a good solution may not be found in a straight-forward way. Fig. 1 shows a topology viewed from the top, where users are surrounded by high buildings. The grid-shaded area represents the double-LOS region $\tilde{\mathcal{D}}_0$ sliced at the altitude H_{\min} . In Fig. 1(a), the double-LOS region is off the middle perpendicular plane between two users when they are behind tall buildings. In Fig. 1(b), the

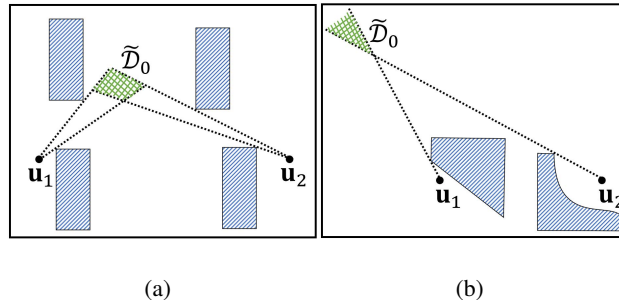


Figure 1. Double-LOS regions sliced at the altitude H_{\min} under building topologies in extreme cases from a top view, where the building height is close to the minimum UAV altitude H_{\min} . (a) $\tilde{\mathcal{D}}_0$ appears off the middle-perpendicular plane between the two users. (b) $\tilde{\mathcal{D}}_0$ appears at the top-left in the region, *i.e.*, could be far away from both users.

double-LOS region can even be far away from the two users when they are surrounded by tall buildings.

Second, the structure of $\tilde{\mathcal{D}}_0$ may lead to arbitrarily many local optima due to possibly a huge number of structures or sub-structures in the urban area of interest. As a result, the approach in [29] which models the environment using polyhedrons is difficult to implement due to the complexity of the environment and the possibly large amount of local optima. This paper, on the contrary, attempts to develop an exploration-exploitation approach with an aim to establish some theoretical guarantees for the global optimality of the UAV position.

III. ALGORITHM FOR THE OPTIMAL SOLUTION ON THE MIDDLE-PERPENDICULAR PLANE

In this section, we solve a simpler version of the problem, where we aim at finding the optimal UAV position on the middle perpendicular plane between the two users. First, two useful properties are investigated for the UAV placement problem constrained on the middle perpendicular plane. Based on these properties, an efficient algorithm is developed. Then, we prove that the algorithm finds the globally optimal UAV position on the 2D middle perpendicular plane with a linear trajectory length.

A. Properties on the Middle-perpendicular Plane

Mathematically, the middle perpendicular plane is specified as $\mathcal{S} = \{\mathbf{p} \in \mathbb{R}^3 : d_1(\mathbf{p}) = d_2(\mathbf{p})\}$, which is a 2D plane passing through the midpoint between the two users at \mathbf{u}_1 and \mathbf{u}_2 and perpendicular to the line connecting the two users. From the definition, one only needs to

focus on minimizing either $d_1(\mathbf{p})$ or $d_2(\mathbf{p})$. This property motivates the search on the middle perpendicular plane.

In addition, recall that the two users are assumed to locate at the ground level, and hence, the middle perpendicular plane is also perpendicular to the ground. As a consequence, there are two additional properties summarized in the following lemmas which make it efficient to explore on the middle perpendicular plane.

The first property is on the double-LOS pattern on the middle perpendicular plane. Define $\tilde{\mathcal{D}}_0^c$ as the set of permissible UAV positions which are *non-double-LOS*.

Lemma 1 (Double-LOS structure on \mathcal{S}). *If $\mathbf{p} \in \mathcal{S} \cap \tilde{\mathcal{D}}_0$, then any $\mathbf{p}' \in \mathcal{S}$ perpendicularly above \mathbf{p} also satisfies $\mathbf{p}' \in \mathcal{S} \cap \tilde{\mathcal{D}}_0$. If $\mathbf{p} \in \mathcal{S} \cap \tilde{\mathcal{D}}_0^c$, then any $\mathbf{p}' \in \mathcal{S}$ perpendicularly below \mathbf{p} also satisfies $\mathbf{p}' \in \mathcal{S} \cap \tilde{\mathcal{D}}_0^c$.*

Proof. The first property follows due to the upward invariant property of $\mathcal{D}_0^{(i)}$ and the fact that \mathcal{S} is perpendicular to the ground. For the second property, assume that \mathbf{p}' is a double-LOS position, *i.e.*, $\mathbf{p}' \in \mathcal{S} \cap \tilde{\mathcal{D}}_0$. Then, according to the upward invariant property, we must have $\mathbf{p} \in \mathcal{S} \cap \tilde{\mathcal{D}}_0$, violating the condition that $\mathbf{p} \in \mathcal{S} \cap \tilde{\mathcal{D}}_0^c$, leading to a contradiction. Therefore, the second property also holds. \square

Lemma 1 can be interpreted as follows: if a position is double-LOS, then all positions perpendicularly above it are double-LOS; on the other hand, if a position is non-double-LOS, then all positions perpendicularly below it are non-double-LOS. An example of the double-LOS pattern on the search plane \mathcal{S} is illustrated in Fig. 2.

The second property leads to a simplified problem for the search constrained on the middle perpendicular plane as follows

$$\begin{aligned} \mathcal{P}' : \quad & \underset{\mathbf{p}}{\text{maximize}} \quad F(\mathbf{p}) \\ & \text{subject to} \quad \mathbf{p} \in \tilde{\mathcal{D}}_0 \cap \mathcal{S}. \end{aligned} \quad (2)$$

Define $\mathbf{o} = \frac{1}{2}(\mathbf{u}_1 + \mathbf{u}_2)$ as the midpoint between the two users. Denote the radius from a point \mathbf{p} on the perpendicular plane \mathcal{S} to the midpoint \mathbf{o} as

$$r(\mathbf{p}) \triangleq \|\mathbf{p} - \mathbf{o}\|_2. \quad (3)$$

Lemma 2 (Optimality with minimum radius). *The solution $\hat{\mathbf{p}}$ to \mathcal{P}' minimizes the radius $r(\mathbf{p})$ subject to $\mathbf{p} \in \tilde{\mathcal{D}}_0 \cap \mathcal{S}$.*

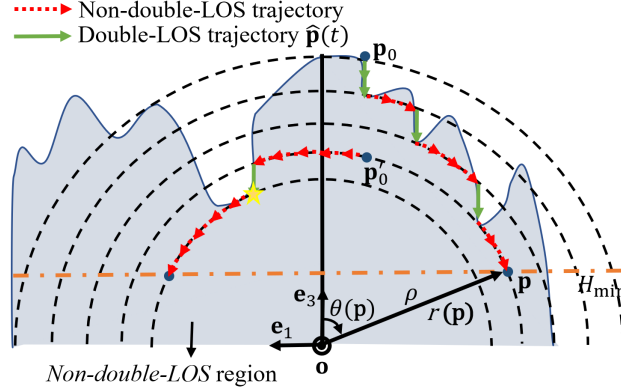


Figure 2. Search trajectory on the middle perpendicular plane from the perspective of \mathbf{u}_2 : flying straight down and along the circle makes $r(\mathbf{p})$ gradually decrease, and correspondingly, the objective value $F(\mathbf{p})$ increases.

Proof. First, note that $d_1(\mathbf{p}) = d_2(\mathbf{p})$ on the middle perpendicular plane. Second, since $f(d)$ is assumed to be decreasing in d , $F(\mathbf{p}) = \min \{f(d_1(\mathbf{p})), f(d_2(\mathbf{p}))\}$ is decreasing in $d_1(\mathbf{p})$. Therefore, maximizing $F(\mathbf{p})$ is equivalent to minimizing $d_1(\mathbf{p})$. Finally, since $d_1(\mathbf{p}) = \|\mathbf{p} - \mathbf{u}_1\|_2 = \sqrt{r(\mathbf{p})^2 + \|\mathbf{u}_1 - \mathbf{o}\|_2^2}$, maximizing $F(\mathbf{p})$ is equivalent to minimizing $r(\mathbf{p})$. \square

Lemma 2 suggests that the optimal position on the middle perpendicular plane \mathcal{S} that solves \mathcal{P}' is the closest double-LOS position to the midpoint \mathbf{o} .

B. Search Algorithm

Using the property of the double-LOS pattern as summarized in Lemma 1, the optimal position on the middle perpendicular plane can be efficiently found following a search trajectory that starts from a double-LOS initial position and repeats the following two steps:

- **Search downward** whenever the UAV is at double-LOS;
- **Search along the circle** with a fixed radius to the midpoint \mathbf{o} whenever the UAV is at non-double-LOS.

We now specify the technical details of the above search strategy using a polar coordinate system (ρ, θ) defined on the middle perpendicular plane \mathcal{S} . Recall that \mathbf{e}_1 is a horizontal basis vector perpendicular to $\mathbf{u}_2 - \mathbf{u}_1$, and \mathbf{e}_3 is a vertical basis vector pointing upward. Using the midpoint \mathbf{o} as the origin, the deviation angle $\theta(\mathbf{p})$ of a position \mathbf{p} with respect to (w.r.t.) the direction \mathbf{e}_3 shown in Fig. 2 is computed as

$$\theta(\mathbf{p}) = \text{sign}(-\mathbf{p}^T \mathbf{e}_1) \arccos(\mathbf{p}^T \mathbf{e}_3 / \|\mathbf{p}\|_2) \quad (4)$$

where $\text{sign}(-\mathbf{p}^T \mathbf{e}_1) = 1$, if $-\mathbf{p}^T \mathbf{e}_1 > 0$, indicating \mathbf{p} on the right quadrant, and $\text{sign}(-\mathbf{p}^T \mathbf{e}_1) = -1$, if $-\mathbf{p}^T \mathbf{e}_1 < 0$, indicating \mathbf{p} on the left quadrant as shown in Fig. 2. As a result, any position \mathbf{p} on the perpendicular plane \mathcal{S} can be expressed using the polar coordinate $(\rho, \theta(\mathbf{p}))$, where $\rho = r(\mathbf{p})$ is defined in (3).

Denote the search position at time t as $\mathbf{p}(t)$. Then, when $\mathbf{p}(t)$ is in non-double-LOS region, the search over an arc with a fixed radius can be specified by the dynamic equation $\rho d\theta = \pm v dt$ in the polar coordinate system (ρ, θ) , where $\rho = r(\mathbf{p}(t))$ and v is the search speed. The detailed algorithm is summarized in Algorithm 1, and an example of search trajectory is shown in Fig. 2.

Note that Algorithm 1 requires a double-LOS initial position \mathbf{p}_0 . Such a position can be found by increasing the altitude of \mathbf{p} until $\mathbf{p} \in \tilde{\mathcal{D}}_0$. This is because for two outdoor users, double-LOS can be guaranteed at a high enough altitude for \mathbf{p} .

Algorithm 1 Dynamic Search Trajectory on the Middle-perpendicular Plane

Input: Initial double-LOS position \mathbf{p}_0 , and search speed v .

Objective: Design the search trajectory $\mathbf{p}(t)$ and record the double-LOS trajectory $\hat{\mathbf{p}}(t)$.

- 1) Initialization: Set $\mathbf{p}(0) = \mathbf{p}_0$ and $\hat{\mathbf{p}}(0) = \mathbf{p}_0$.
 - 2) **Clockwise search:**
 - a) If $\mathbf{p}(t) \in \tilde{\mathcal{D}}_0$ then
 - i) Set $\hat{\mathbf{p}}(t) = \mathbf{p}(t)$.
 - ii) Decrease the altitude of $\mathbf{p}(t)$ according to $dp_3(t) = -v dt$.
 - b) Else
 - i) $\hat{\mathbf{p}}(t)$ remains unchanged, *i.e.*, $d\hat{\mathbf{p}}(t) = 0$.
 - ii) Move along the circle according to the dynamical equation: $\rho d\theta = v dt$ expressed in the polar coordinate system (ρ, θ) , where $\rho = r(\mathbf{p}(t))$.
 - c) Repeat Step 2a and 2b until the altitude of $\mathbf{p}(t)$ drops to H_{\min} .
 - 3) Define a second initial point \mathbf{p}'_0 below \mathbf{p}_0 that satisfies $r(\mathbf{p}'_0) = r(\hat{\mathbf{p}}(t))$ and $(\mathbf{p}_0 - \mathbf{p}'_0) / \|\mathbf{p} - \mathbf{p}'_0\|_2 = \mathbf{e}_3$. Set $\mathbf{p}(t) = \mathbf{p}'_0$ and $\hat{\mathbf{p}}(t)$ remains unchanged.
 - 4) **Anticlockwise search:** Repeat Step 2, but replace the dynamical equation in Step 2(b)ii as $\rho d\theta = -v dt$, until the altitude of $\mathbf{p}(t)$ again drops to H_{\min} .
-

C. Optimality and Complexity of the Search on \mathcal{S}

It turns out that Algorithm 1 finds the globally optimal solution to \mathcal{P}' despite that the double-LOS region $\tilde{\mathcal{D}}_0$ can be arbitrarily complicated.

Theorem 1 (Global optimality in 2D). *The double-LOS trajectory $\hat{\mathbf{p}}(t)$ of Algorithm 1 terminates at the globally optimal solution to \mathcal{P}' .*

Proof. See Appendix A. □

Theorem 1 asserts that the global optimality on the 2D middle perpendicular plane can be guaranteed by a continuous search trajectory which can be adaptively determined by one of the following two dynamical equations: $dp_3(t) = -vdt$ and $\rho d\theta = \pm vdt$, according to the double-LOS status discovered along the trajectory.

In addition, the length of the search trajectory is upper bounded as shown in the following proposition.

Proposition 1 (Maximum trajectory length). *Denote $R_0 = r(\mathbf{p}_0)$ as the radius of the initial double-LOS point \mathbf{p}_0 , and H_0 is the altitude of \mathbf{p}_0 . The length of the search trajectory of Algorithm 1 is upper bounded by $2(H_0 - H_{\min}) + \pi R_0$.*

Proof. When the UAV is in double-LOS region, it searches downwards. The total length of straight down steps is upper bounded by $2(H_0 - H_{\min})$. When the UAV is in non-double-LOS region, it searches along a circle whose radius is upper bounded by R_0 , and correspondingly, the total length of these arc-shape steps are upper bounded by πR_0 . Therefore, the upper bound of the total length of the trajectory is given by $2(H_0 - H_{\min}) + \pi R_0$. □

Two observations are made from Theorem 1 and Proposition 1. First, to guarantee a globally optimal solution on the 2D middle perpendicular plane \mathcal{S} , it only requires a search complexity to be a linear function of the initial distance R_0 and the initial height H_0 , regardless of the actual structure of the double-LOS region $\tilde{\mathcal{D}}_0$. This is due to the fact that Algorithm 1 has exploited the upward invariant property of the double-LOS pattern as summarized in Lemma 1.

Second, the fact that the globally optimal solution in 2D is theoretically guaranteed is also due to the continuous search trajectory where one needs to determine the double-LOS status for each $\mathbf{p}(t)$ with an infinitesimal step size dt as described in Algorithm 1. Nevertheless, in a more

practical setting in our numerical experiments, a step size of 5 meters is adopted and the global optimality in 2D is still numerically observed as shown in Section V.

IV. SEARCH FOR THE OPTIMAL SOLUTION IN 3D

In this section, we aim at searching for the globally optimal solution in 3D for problem \mathcal{P} by exploring a bounded 2D area.

Denote the set of permissible UAV positions as \mathcal{P} . Denote the critical distance $d_0(\mathbf{p}) = \max\{d_1(\mathbf{p}), d_2(\mathbf{p})\}$ as the longer distance from the UAV position \mathbf{p} to the two users. Given an initial double-LOS point \mathbf{p}_0 in \mathcal{P} , define a region

$$\mathcal{B}(\mathbf{p}_0) = \{\mathbf{p} \in \mathcal{P}: d_0(\mathbf{p}) \leq d_0(\mathbf{p}_0)\}$$

which geometrically appears as a cap.

It follows that the globally optimal solution \mathbf{p}^* to \mathcal{P} must lie in the cap $\mathcal{B}(\mathbf{p}_0)$. To see this, since $f(d)$ is decreasing in d , the objective function $F(\mathbf{p}) = \min\{f(d_1(\mathbf{p})), f(d_2(\mathbf{p}))\}$ must also be decreasing in the critical distance $d_0(\mathbf{p})$. Since \mathbf{p}_0 is a feasible solution and, by definition, any point $\mathbf{p} \notin \mathcal{B}(\mathbf{p}_0)$ has a critical distance $d_0(\mathbf{p})$ greater than $d_0(\mathbf{p}_0)$, implying that the optimal solution cannot be outside $\mathcal{B}(\mathbf{p}_0)$.

Next, we will narrow down the search area from the 3D cap $\mathcal{B}(\mathbf{p}_0)$ to bounded 2D areas by algebraically deriving the solution under several typical LOS patterns.

A. A Compact Search Area on the Perpendicular Plane

It turns out that it suffices to search on the middle perpendicular plane \mathcal{S} to reveal the LOS status of the majority part of the cap $\mathcal{B}(\mathbf{p}_0)$. The key idea is to map the LOS status from a point in $\mathcal{B}(\mathbf{p}_0)$ to a point on \mathcal{S} using the colinear invariant property of the LOS regions $\mathcal{D}_0^{(i)}$ for each user i . Specifically, given a point $\mathbf{p} \in \mathcal{B}(\mathbf{p}_0)$, to investigate the LOS status for the i th user, find a point \mathbf{p}_i on the middle perpendicular plane \mathcal{S} , such that the three points \mathbf{u}_i , \mathbf{p}_i , and \mathbf{p} are colinear as illustrated in Fig 3. As a result, according to the colinear invariant property, \mathbf{p} and \mathbf{p}_i share the same LOS status for user i .

However, it is still very challenging to determine the double-LOS status for \mathbf{p} , because one needs to visit two separate locations, \mathbf{p}_1 and \mathbf{p}_2 , as shown in Fig. 3, to determine the LOS status for the two users, respectively. Thus, the key is how to efficiently combine the LOS information for the two users along a simple search trajectory.

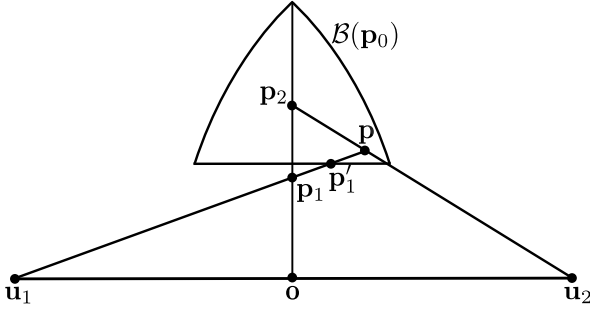


Figure 3. Region $\mathcal{B}(\mathbf{p}_0)$: The LOS status to \mathbf{u}_1 of a point $\mathbf{p} \in \mathcal{B}(\mathbf{p}_0)$ can be determined by that of $\mathbf{p}_1 \in \mathcal{S}$ or $\mathbf{p}'_1 \in \mathcal{H}$.

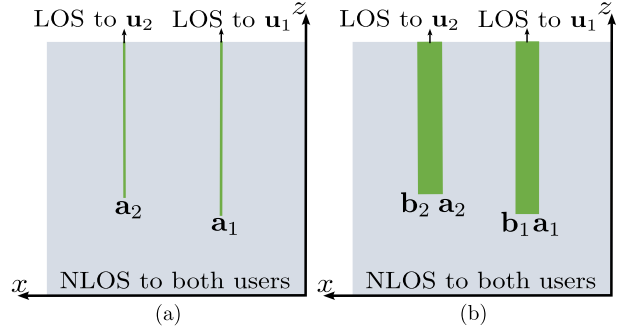


Figure 4. (a) double-ray LOS pattern; (b) double-stripe LOS pattern

The first step that we tackle this issue is to develop the closed-form expression of the globally optimal solution under the simplest LOS pattern.

1) Double-ray LOS Pattern: Consider two points $\mathbf{a}_1, \mathbf{a}_2 \in \mathcal{S}$ on the middle perpendicular plane, where \mathbf{a}_1 and \mathbf{a}_2 are LOS positions of user 1 and user 2, respectively. According to the upward invariant property of the LOS regions, the positions perpendicularly above \mathbf{a}_1 and \mathbf{a}_2 are also LOS for user 1 and user 2, respectively, as shown in Fig. 4(a).

Suppose that the LOS regions on the middle perpendicular plane $\mathcal{D}_0^{(i)} \cap \mathcal{S}$ are given by the above double-ray pattern, where the two rays do not overlap. It is clear that there is no solution on the middle perpendicular plane, but there could be a solution off the middle perpendicular plane, and the globally optimal solution \mathbf{p}^* to problem \mathcal{P} can be computed as follows.

Proposition 2 (Double-ray LOS Pattern). *Suppose that the set of LOS positions $\mathcal{D}_0^{(1)} \cap \mathcal{S}$ of user 1 is a perpendicular ray with a lowest point $\mathbf{a}_1 = (a_{11}, a_{12}, a_{13})$. The set of LOS positions $\mathcal{D}_0^{(2)} \cap \mathcal{S}$ of user 2 is another perpendicular ray with a lowest point $\mathbf{a}_2 = (a_{21}, a_{22}, a_{23})$. If $a_{11}a_{21} > 0$, then the globally optimal solution \mathbf{p}^* to \mathcal{P} is given by*

$$\mathbf{q}(\mathbf{a}_1, \mathbf{a}_2) = \begin{cases} \frac{2a_{21}}{a_{11}+a_{21}}\mathbf{a}_1 - \frac{L}{2}\mathbf{e}_2, & \text{if } \frac{a_{13}}{a_{23}} > \frac{a_{11}}{a_{21}} \\ \frac{2a_{11}}{a_{11}+a_{21}}\mathbf{a}_2 + \frac{L(a_{21}-2a_{11})}{2a_{11}}\mathbf{e}_2, & \text{otherwise} \end{cases} \quad (5)$$

where $\mathbf{e}_2 = (\mathbf{u}_2 - \mathbf{u}_1) / \|\mathbf{u}_2 - \mathbf{u}_1\|_2$, and $L = \|\mathbf{u}_2 - \mathbf{u}_1\|_2$.

Proof. See Appendix B. □

Naturally, any LOS pattern on the search plane can be modeled as a union of double-ray LOS patterns parameterized by the endpoints $(\mathbf{a}_1, \mathbf{a}_2)$. Thus, we extend the result to the case of

double-stripe LOS pattern as follows.

2) Double-stripe LOS pattern: Consider two LOS vertical regions with horizontal bottom line segments $\overline{A_1B_1}$, and $\overline{A_2B_2}$. Denote the coordinates of the endpoints of the line segment $\overline{A_iB_i}$ as $\mathbf{a}_i = (a_{i1}, a_{i2}, h_i)$ and $\mathbf{b}_i = (b_{i1}, b_{i2}, h_i)$, respectively. Without loss of generality, suppose that $|a_{i1}| \leq |b_{i1}|$, $a_{i1}b_{i1} > 0$, and $h_i \geq H_{\min}$ for $i \in \{1, 2\}$. Note that positions above $\overline{A_iB_i}$ are LOS w.r.t. user i , according to the upward invariant property, as shown in Fig. 4(b).

The double-stripe LOS pattern can be constructed as a union of many double-ray LOS patterns. As a result, if the LOS regions $\mathcal{D}_0^{(i)} \cap \mathcal{S}$ on the middle perpendicular plane \mathcal{S} appear as a double-stripe LOS pattern, Proposition 2 implies that problem \mathcal{P} can be equivalently reformulated as

$$\begin{aligned} \mathcal{P}'' : \underset{\mathbf{p}}{\text{maximize}} \quad & F(\mathbf{p}) \\ \text{subject to} \quad & \mathbf{p} = \mathbf{q}(\mathbf{x}_1, \mathbf{x}_2) \\ & \min \{a_{i1}, b_{i1}\} \leq x_{i1} \leq \max \{a_{i1}, b_{i1}\} \\ & x_{i2} = a_{i2}, x_{i3} = h_i, \text{ for } i = 1, 2. \end{aligned} \tag{6}$$

It is found that problem \mathcal{P}'' has a closed-form expression (14) as derived in Appendix C. The fact that \mathcal{P}'' has a closed-form solution can be understood from the following two aspects. First, the objective function $F(\mathbf{p})$ is monotonically decreasing in $d_0(\mathbf{p})$, the longer distance from \mathbf{p} to the two users. Thus, the objective is equivalent to minimizing $d_0(\mathbf{p})$, a locally convex function of \mathbf{p} in the regions of $\{\mathbf{p} \in \mathcal{P} : d_1(\mathbf{p}) < d_2(\mathbf{p})\}$ or $\{\mathbf{p} \in \mathcal{P} : d_1(\mathbf{p}) > d_2(\mathbf{p})\}$. Second, from (5) and (6), the constraint set can be decomposed into a union of several rectangles. Thus, the intermediate variables \mathbf{x}_1 and \mathbf{x}_2 , in $\mathbf{p} = \mathbf{q}(\mathbf{x}_1, \mathbf{x}_2)$, must be found at the endpoints of the intervals $(\mathbf{a}_i, \mathbf{b}_i)$. As a result, the closed-form solution (14) is derived via a case-by-case discussion for a total of eight cases.

Denote $Q(\mathbf{a}_1, \mathbf{b}_1; \mathbf{a}_2, \mathbf{b}_2)$ as the solution to \mathcal{P}'' , which is also the solution to \mathcal{P} , under the double-stripe LOS pattern. With the closed-form solution $Q(\mathbf{a}_1, \mathbf{b}_1; \mathbf{a}_2, \mathbf{b}_2)$ to \mathcal{P} , one can design simple search trajectories to collect the endpoints $(\mathbf{a}_i, \mathbf{b}_i)$, $i \in \{1, 2\}$ of LOS segments for both users, to find the best double-LOS position as will be discussed in Section IV-D.

B. A Compact Search Area on the Horizontal Plane

The search on the perpendicular search plane \mathcal{S} has limitations, because the search height cannot be lower than H_{\min} due to the problem constraint.¹ For a point \mathbf{p} that leads to a colinear

¹Recall that, in practice, there could be collision with buildings if the search altitude of the UAV is not lower bounded.

point $\mathbf{p}_1 \in \mathcal{S}$, *i.e.*, \mathbf{p}_1 , \mathbf{u}_1 , and \mathbf{p} are colinear, with altitude lower than H_{\min} as shown in Fig. 3, the point \mathbf{p}_1 cannot be reached by the search trajectory on \mathcal{S} , and hence, the LOS status of \mathbf{p} w.r.t. \mathbf{u}_1 cannot be inferred from \mathbf{p}_1 .

The remedy to such a limitation is to find another colinear point \mathbf{p}'_1 on the horizontal plane $\mathcal{H} = \{(x, y, z) : z = H_{\min}\}$, such that \mathbf{u}_1 , \mathbf{p}_1 , \mathbf{p}'_1 , and \mathbf{p} are colinear. Given \mathbf{p}'_1 , the coordinates of point \mathbf{p}_1 are calculated as

$$\mathbf{p}_1 = T_1(\mathbf{p}'_1) \triangleq \frac{L}{2(p'_{12} + L/2)}(\mathbf{p}'_1 - \mathbf{u}_1) + \mathbf{u}_1. \quad (7)$$

Then, according to the colinear invariant property of the LOS regions, \mathbf{p} is LOS from \mathbf{u}_1 only if \mathbf{p}_1 and \mathbf{p}'_1 are LOS from \mathbf{u}_1 . As a result, one can search on \mathcal{H} to discover the LOS opportunity for \mathbf{p} .

Similarly, the LOS status of point \mathbf{p}_2 w.r.t. \mathbf{u}_2 can be revealed by the colinear point \mathbf{p}'_2 , *i.e.*,

$$\mathbf{p}_2 = T_2(\mathbf{p}'_2) \triangleq \frac{L}{2(-p'_{22} + L/2)}(\mathbf{p}'_2 - \mathbf{u}_2) + \mathbf{u}_2. \quad (8)$$

Combining the two search strategies, we have the following results.

Lemma 3 (Compact 2D Search Areas). *Given a double-LOS initial point \mathbf{p}_0 , define $\tilde{\mathcal{B}}(\mathbf{p}_0) = \mathcal{B}(\mathbf{p}_0)$, if $d_0(\mathbf{p}_0) \leq \sqrt{2}L/2$ or $d_0(\mathbf{p}_0) \geq L$, and $\tilde{\mathcal{B}}(\mathbf{p}_0) = \{\mathbf{p} \in \mathcal{P} : d_0(\mathbf{p}) < L^2 / (2\sqrt{L^2 - d_0^2(\mathbf{p}_0)})\}$, otherwise. Then, the optimal solution to \mathcal{P} can be found by searching the LOS points in $\tilde{\mathcal{B}}(\mathbf{p}_0) \cap \mathcal{S}$ and $\tilde{\mathcal{B}}(\mathbf{p}_0) \cap \mathcal{H}$.*

Proof. See Appendix D. □

Lemma 3 reveals two important properties. First, given a double-LOS initial point, the search for the globally optimal position can be reduced from possibly an 3D unbounded area to a bounded area $\tilde{\mathcal{B}}(\mathbf{p}_0)$. Second, for the 3D globally optimal solution, it suffices to search on a bounded 2D area $\tilde{\mathcal{B}}(\mathbf{p}_0) \cap \mathcal{S}$ and $\tilde{\mathcal{B}}(\mathbf{p}_0) \cap \mathcal{H}$.

C. A Theoretical Bound to the Global Optimality under a Naive Trajectory

Lemma 3 still requires to search over a bounded 2D area for the globally optimal solution to \mathcal{P} . However, in practice, the UAV can only explore through a 1D trajectory. Therefore, a key question is whether there exists a set of search trajectories with finite length that guarantee to find a suboptimal solution, with a performance gap to that of the globally optimal one upper bounded by a given value.

To answer the above question, we study a set of *naive* trajectories as follows. Denote $H_0 = \sqrt{d_0^2(\mathbf{p}_0) - L^2/4}$ as the height at the top of the cap $\mathcal{B}(\mathbf{p}_0)$, and $H'_{\min}(\mathbf{p}_0) = LH_{\min}/(2\sqrt{d_0^2(\mathbf{p}_0) - H_{\min}^2})$ as the minimum height for \mathbf{p}_1 to reach the LOS status for every $\mathbf{p} \in \mathcal{B}(\mathbf{p}_0)$ as shown in Fig. 3. Define an effective search region $\mathcal{B}'(\mathbf{p}_0) \cap \mathcal{S}$, where $\mathcal{B}'(\mathbf{p}_0) \triangleq \{\mathbf{p} \in \mathbb{R}^3 : p_3 \geq H'_{\min}(\mathbf{p}_0), d_0(\mathbf{p}) \leq d_0(\mathbf{p}_0)\}$. Consider a set of equally-spaced search trajectories $\mathcal{T} \in \mathcal{B}'(\mathbf{p}_0) \cap \mathcal{S}$ parallel to the ground with heights given by $h_j = H_0 - j\delta$, where δ is the step size in altitude between adjacent horizontal trajectories, and $j = 1, 2, \dots, \lfloor (H_0 - H'_{\min}(\mathbf{p}_0))/\delta \rfloor$. Note that for $H'_{\min}(\mathbf{p}_0) \leq h_j < H_{\min}$, the LOS status of \mathbf{p}_i on \mathcal{S} needs to be inferred by searching \mathbf{p}'_i on \mathcal{H} as given in (7) and (8).

As a result, the LOS information collected along the trajectory \mathcal{T} appears as a set of LOS intervals $\mathcal{I}_1 \triangleq \mathcal{T} \cap \mathcal{D}_0^{(1)}$ and $\mathcal{I}_2 \triangleq \mathcal{T} \cap \mathcal{D}_0^{(2)}$, which are one-dimensional subsets of the LOS regions $\mathcal{D}_0^{(1)}$ and $\mathcal{D}_0^{(2)}$. Therefore, a suboptimal solution can be found by solving a set of problems \mathcal{P}'' parameterized by the LOS intervals $\{(\mathbf{a}_1, \mathbf{b}_1)\}$ collected in \mathcal{I}_1 and $\{(\mathbf{a}_2, \mathbf{b}_2)\}$ in \mathcal{I}_2 , and picking the best solution. Mathematically, this is formulated in the following problem

$$\begin{aligned}
& \underset{\mathbf{p}}{\text{maximize}} && F(\mathbf{p}) \\
& \text{subject to} && \mathbf{p} = Q(\mathbf{a}_1, \mathbf{b}_1; \mathbf{a}_2, \mathbf{b}_2) \\
& && (\mathbf{a}_1, \mathbf{b}_1) \in \mathcal{I}_1 \\
& && (\mathbf{a}_2, \mathbf{b}_2) \in \mathcal{I}_2.
\end{aligned} \tag{9}$$

Let $\tilde{\mathbf{p}}$ be the solution to (9). Then, if $d_0(\tilde{\mathbf{p}}) \leq \sqrt{2}L/2$, it is found that the gap to the globally optimal solution \mathbf{p}^* to \mathcal{P} is bounded linearly in δ , the vertical step size between adjacent trajectories.

Theorem 2 (Performance Gap to the Globally Optimal Solution). *If the solution $\tilde{\mathbf{p}}$ to (9) satisfies $d_0(\tilde{\mathbf{p}}) \leq \sqrt{2}L/2$, then, the performance gap to the globally optimal solution \mathbf{p}^* is upper bounded as*

$$d_0(\tilde{\mathbf{p}}) - d_0(\mathbf{p}^*) \leq 2\delta\sqrt{d_0^2(\tilde{\mathbf{p}}) - H_{\min}^2}/L. \tag{10}$$

Moreover, if $f(d)$ is convex, then $F(\mathbf{p}^*) - F(\tilde{\mathbf{p}}) \leq -2\delta f'(d_0(\mathbf{p}^*))\sqrt{d_0^2(\tilde{\mathbf{p}}) - H_{\min}^2}/L$.

Proof. See Appendix E. □

Theorem 2 finds that, searching over a set of vertically δ -spaced parallel trajectories, if the solution computed from (9) satisfies $d_0(\tilde{\mathbf{p}}) \leq \sqrt{2}L/2$, then it is guaranteed that the gap to the

global optimality is $O(\delta)$. One can further compute that the coefficient $2\sqrt{d_0^2(\tilde{\mathbf{p}}) - H_{\min}^2}/L$ in (10) is upper bounded as 1.4, *i.e.*, $d_0(\tilde{\mathbf{p}}) - d_0(\mathbf{p}^*) \leq 1.4\delta$. In addition, the upper bound of the total length of the search trajectories in \mathcal{T} can be found upper bounded by $2H_0\sqrt{H_0^2 - H_{\min}^2}/\delta$ via the total bounded search area divided by the vertical step size δ . This implies that the total length of the search trajectory is $O(1/\delta)$.

D. A Dynamic Multi-stage Algorithm

Inspiring from Theorem 2, an efficient search trajectory can be developed. Specifically, the following properties derived from the theoretical bound $O(\delta)$ in Theorem 2 can be exploited. First, a dynamic multi-stage search can be developed, where one first performs a coarse global search to identify promising regions, and then, narrow down the search region in subsequent stages for finer search. Specifically, consider to perform an M -stage search. The first stage follows $(2^{M-1}\delta)$ -spaced parallel trajectories represented by the red lines in Fig. 5. Then, define the *critical trajectories* as the line segments lying between an LOS segment of a trajectory and an NLOS trajectory, for example, the solid green lines in Fig. 5. According to the upward invariant property, in the next stage, it suffices to search those critical trajectories for the fine-grained LOS information. Using such a search strategy, it can be found that the total length of the critical trajectories in an M -stage search is upper bounded as $2H_0\sqrt{H_0^2 - H_{\min}^2}/(2^{M-1}\delta) + 2(M-1)\sqrt{H_0^2 - H_{\min}^2}$, which is minimized at $M = g_W(H_0 \ln 2/\delta)/\ln 2$, where $g_W(x)$ is the Lambert W function of x . We find that in a typical setting, *e.g.*, $H_0 \in [120, 160]$ meters and $\delta \in [2, 3]$ meters, the optimal M is 4.

Second, the $O(\delta)$ bound helps filter out unpromising region for subsequent finer search using the coarse LOS information obtained at the previous stages. For example, if $\tilde{\mathbf{p}}_1$ and $\tilde{\mathbf{p}}_2$ are both found as double-LOS points with $d_0(\tilde{\mathbf{p}}_2) - d_0(\tilde{\mathbf{p}}_1) > 2^{M-m+1}\delta\sqrt{d_0^2(\tilde{\mathbf{p}}_2) - H_{\min}^2}/L$, then there is no need to finely search the local area related to $\tilde{\mathbf{p}}_2$, because of the $O(\delta)$ upper bound in Theorem 2. For example, the dashed green critical trajectory in Fig. 5 may be ignored if it is found substantially less promising than the other critical trajectories in solid green.

Finally, there exist path planning algorithms to connect the isolated critical trajectories using a short path. The overall search strategy is summarized in Algorithm 2, and an typical realization of the trajectory is demonstrated in Fig. 5, where the target search region is reduced stage-by-stage.

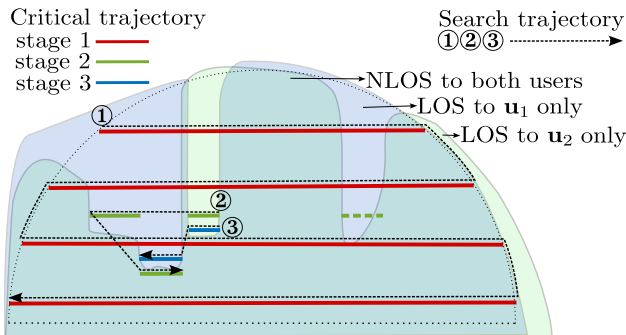


Figure 5. An example of search trajectory on $\mathcal{B}(\mathbf{p}_0) \cap \mathcal{S}$: The bold solid line represents the critical trajectory. The thin dashed lines with arrows indicate a search trajectory to connect the critical trajectories at different stages ($m = 1, 2, 3$). The light green and light blue shaded areas portray the NLOS patterns to user 1 and user 2, respectively. The overlapping region of the two NLOS patterns is NLOS to both users.

V. NUMERICAL RESULTS

In this section, the proposed algorithms are compared with four baseline schemes on four real-world city maps.

A. Environment Setup and Scenarios

We perform experiments over four city topologies from real data. As shown in Fig. 6, Map A and Map B are 3D maps of two different areas in Beijing, China. They represent the 3D environment of typical commercial center and traditional commercial area, respectively. Map C and Map D are 2D street maps of two different areas in Guangzhou, China. Based on the street maps, we manually generate the height of the buildings following a uniform distribution of $[50, 80]$ meters. The two simulated environments respectively represent the modern dense residential area and the ultra dense area probably appear in the future.

The characteristics of the four maps are summarized in Table I, where we use the building coverage ratio (BCR) and floor area ratio (FAR) [31] to quantify the building density of the areas. It is observed that Map A is the most sparse, and Map D has the largest building density.

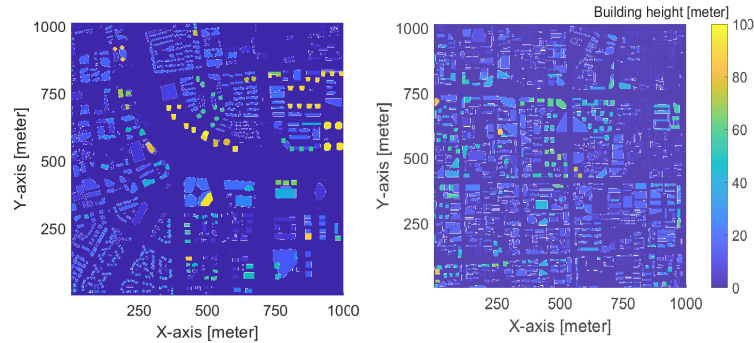
For the experiment on each map, the minimum height of the UAV H_{\min} is set as the maximum building height in the map, as shown in Table I, to avoid potential collision of the UAV. There are 5,000 user pairs placed uniformly at random in the non-building area of each map.

Two application scenarios are evaluated in our experiments.

Algorithm 2 M -stage Dynamic Search for 3D Optimal UAV Placement

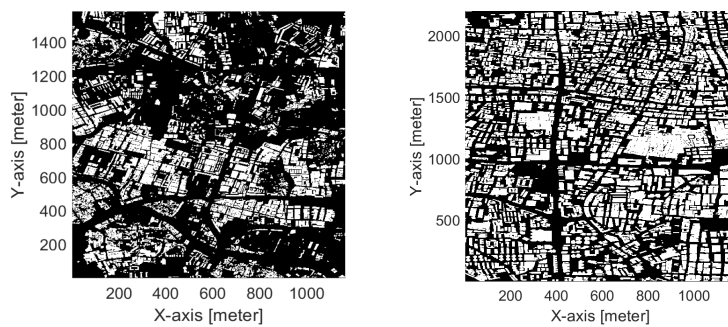
- 1) Initialization: Based on a double-LOS initial point \mathbf{p}_0 , set the initial solution $\tilde{\mathbf{p}}(1) = \mathbf{p}_0$. Initialize $\mathcal{I}_1 = \emptyset$, $\mathcal{I}_2 = \emptyset$, $H_0 = \sqrt{d_0^2(\mathbf{p}_0) - L^2/4}$, $H'_{\min}(\tilde{\mathbf{p}}(1)) = LH_{\min}/(2\sqrt{d_0^2(\tilde{\mathbf{p}}(1)) - H_{\min}^2})$, $j = 1$, and $m = 1$.
 - 2) Set $h_j = H_0 - j2^{M-m}\delta$, for a step size δ . Initialize $\mathcal{I}_i^{(j)} = \emptyset$.
 - 3) **Configure the initial search trajectory.**
 - a) If $h_j \geq H_{\min}$: Search on \mathcal{S} with height h_j between $x = \pm\sqrt{d_0^2(\tilde{\mathbf{p}}(m)) - L^2/4 - h_j^2}$. For any LOS segment discovered for user i with endpoints \mathbf{a}_i and \mathbf{b}_i , assign $(\mathbf{a}_i, \mathbf{b}_i) \rightarrow \mathcal{I}_i^{(j)}$.
 - b) If $h_j < H_{\min}$: Search on \mathcal{H} with $y = L/2 \pm (H_{\min}/h_j - 1)L/2$ between $x = \pm\sqrt{d_0^2(\tilde{\mathbf{p}}(m)) - H_{\min}^2 - L^2H_{\min}^2/(4h_j^2)}$. For any LOS segment discovered for user i with endpoints \mathbf{a}_i and \mathbf{b}_i , assign $(T_i(\mathbf{a}_i), T_i(\mathbf{b}_i)) \rightarrow \mathcal{I}_i^{(j)}$ where T_i for $i = 1, 2$ are given in (7) and (8).
 - c) $\mathcal{I}_i = \mathcal{I}_i \cup \mathcal{I}_i^{(j)}$, $j \leftarrow j + 1$, Repeat from Step 2 until $h_j < H'_{\min}(\tilde{\mathbf{p}}(m))$.
 - 4) Calculate $\tilde{\mathbf{p}}(m)$ as the solution to problem (9).
 - 5) For the k th interval $(\mathbf{a}_i^{(k)}, \mathbf{b}_i^{(k)})$ in \mathcal{I}_i where $k \in \{1, 2, \dots, |\mathcal{I}_i|\}$ and $i \in \{1, 2\}$, calculate the solution $\tilde{\mathbf{p}}_i^{(k)}$ to problem (9) by replacing \mathcal{I}_i with $\{(\mathbf{a}_i^{(k)}, \mathbf{b}_i^{(k)})\}$. If $d_0(\tilde{\mathbf{p}}_i^{(k)}) - d_0(\tilde{\mathbf{p}}(m)) > 2^{M-m+1}\delta\sqrt{d_0^2(\tilde{\mathbf{p}}_i^{(k)}) - H_{\min}^2}/L$, then remove $(\mathbf{a}_i^{(k)}, \mathbf{b}_i^{(k)})$ from \mathcal{I}_i .
 - 6) Reset $j = 1$, and update $m \leftarrow m + 1$.
 - 7) **Configure the refined search trajectory.**
 - a) For each interval $(\mathbf{a}_i, \mathbf{b}_i)$ in \mathcal{I}_i , set $H_0 = a_{i3}$, and repeat from Step 2, but change the range of x in Step 3a as $[a_{i1}, b_{i1}]$ and in Step 3b as $[a_{i1}H_{\min}/a_{i3}, b_{i1}H_{\min}/b_{i3}]$, until $h_j < H_0 - 2^{M-m}\delta$.
 - b) Repeat Step 7a until $m = M$, and then, output $\tilde{\mathbf{p}}(M)$.
-

- **UAV relaying:** A UAV is placed to establish LOS relay channels for two ground users under decode-and-forward relaying. Consider the path loss model of millimeter wave cellular reported in [30] as $\text{PL}_{\text{LOS}}(d) = 61.4 + 20.0 \log_{10}(d)$ with the shadowing parameter $\sigma_{\text{sf}} = 1$ dB for LOS link, and $\text{PL}_{\text{NLOS}}(d) = 72.0 + 29.2 \log_{10}(d)$ with $\sigma_{\text{sf}} = 5$ dB for NLOS link at a carrier frequency of 28 GHz. Correspondingly, the performance evaluation function is defined as the channel capacity $f(d) = W \log(1 + P \cdot 10^{(-\text{PL}(d) - \sigma_{\text{sf}})/10}) / (WN_0)$ where $W = 1$ GHz is the allocated bandwidth, P is the transmission power, and N_0 is the noise



(a) Map A: Typical commercial cen- (b) Map B: Traditional commercial area

ter



(c) Map C: Dense residential area (d) Map D: Ultra dense area

Figure 6. Four local areas, where Map A and B are 3D city maps of different areas in Beijing, China, and Map C and D are generated from 2D street maps from Guangzhou, China, with simulated building heights.

power spectrum density set as -169 dBm/Hz.

- **UAV WPT:** A UAV is placed to wirelessly charge two ground users simultaneously. The evaluation function $f(d)$ of the WPT channel is adopted from the linear harvesting model as $f(d) = \eta P \beta / d^\alpha$ where $\eta = 60\%$ denotes the linear RF-to-direct current (DC) energy conversion efficiency, $P = 40$ dBm denotes the transmit power, $\beta = -30$ dB denotes the channel power gain at reference distance $d_0 = 1$ meter, and $\alpha = 3$ denotes the path loss exponent [32].

We evaluate the following baseline schemes for performance benchmarking. The exhaustive search schemes are implemented using a 5-meter step size.

- *Exhaustive 3D search:* This scheme performs an exhaustive search in the 3D search space above the area of interest.
- *Exhaustive 2D search (horizontal)* [33]: This scheme performs an exhaustive search over a

Table I
MAPS WITH FOUR TYPES OF FUNCTION AREAS

Map	BCR	FAR	Mean height [meter]	Maximum height [meter]	Comment
Map A (Beijing)	19%	1.4	22	96	Typical commercial center
Map B (Beijing)	32%	1.8	16	87	Traditional commercial area
Map C (Guangzhou)	22%	4.9	65	80	Dense residential area
Map D (Guangzhou)	40%	8.8	65	80	Ultra dense area

2D horizontal plane $\{\mathbf{p} \in \mathbb{R}^3 : p_3 = H_{2D}\}$ where H_{2D} is set as 120 meters here.

- *Exhaustive 2D search (vertical)*: This scheme is designed to confirm the optimality of the output of Algorithm 1 on the middle perpendicular plane \mathcal{S} . It performs an exhaustive search over the 2D middle perpendicular plane \mathcal{S} .
- *Statistical method* [17, 23, 34]: The average path loss from the UAV position \mathbf{p} to the i th ground user can be formulated as

$$PL_{\text{ave}} = P_{\text{LOS}}(\mathbf{p}) \times PL_{\text{LOS}}(d_i(\mathbf{p})) + (1 - P_{\text{LOS}}(\mathbf{p}))PL_{\text{NLOS}}(d_i(\mathbf{p})) \quad (11)$$

where $P_{\text{LOS}}(\mathbf{p})$ is the LOS probability of the UAV position \mathbf{p} . The LOS probability $P_{\text{LOS}}(\mathbf{p})$ is defined as

$$P_{\text{LOS}}(\mathbf{p}) = \frac{1}{1 + a \times \exp(-b(\arctan(p_3/r_i) - a))} \quad (12)$$

where $r_i = \sqrt{\|\mathbf{p} - \mathbf{u}_i\|_2^2 - p_3^2}$, and the environmental parameter pair (a, b) is learned from the actual distribution of LOS regions, and obtained as $(2.60, 0.05)$, $(58.91, 8.90)$, $(63.77, 3.95)$, and $(64.33, 141.17)$ in Maps A, B, C, and D, respectively.

B. UAV Communication Relaying

Fig. 7 summarizes the mean capacity of different schemes on the four maps under transmission power $P = 30$ dBm. The numerical result in Fig. 7 confirms the global optimality of Algorithm 1 on the perpendicular plane \mathcal{S} . The mean capacity of Algorithm 1 and exhaustive 2D search on \mathcal{S} is the same as each other in the four function areas. It is worth noting that the trajectory length of Algorithm 1 is at most 1/45 of that of the Exhaustive 2D search on \mathcal{S} as shown in Table II. Thus, Algorithm 1 is much more efficient than the Exhaustive 2D search on \mathcal{S} .

In Map A and B, where the distribution of buildings is relatively sparse, both of the two proposed algorithms achieve mostly the globally optimal performance with a negligible performance gap to the Exhaustive 3D scheme as shown in Fig. 7, although Algorithm 1 only searches on the middle perpendicular plane with limited search length. Such a result suggests that the globally optimal solution has a high chance to locate on the middle perpendicular plane over a sparse city topology.

In Map C and D, where buildings are denser, the performance of Algorithm 1 degrades and it achieves only 85.4% on Map C and 75.2% on Map D to the Exhaustive 3D scheme in Fig. 7. By contrast, the performance of Algorithm 2 with $\delta = 3$ meters is still close, *i.e.*, above 99.8% in Map C and above 98.0% in Map D, to that of the Exhaustive 3D scheme. This is because Algorithm 2 is capable of discovering those potentially better LOS positions off the middle perpendicular plane using coarse LOS information on a bounded 2D region. However, the performance of the statistical method is relatively poor since this method does not examine the actual obstacle occlusion, resulting in no LOS guarantee in practical applications.

Fig. 8 illustrates the average capacity versus the transmission power. For a sparse city topology (Map A), both of the proposed algorithms achieve almost identical performance to the Exhaustive 3D scheme. For a dense topology (Map C), Algorithm 1 degrades from the Exhaustive 3D scheme, but the performance degradation is small at the high transmission power regime. Specifically, Algorithm 1 achieves above 90% to the Exhaustive 3D scheme under transmission power of 40 dBm. In contrast, Algorithm 2 achieves above 99.7% to the Exhaustive 3D scheme at different transmission powers under $\delta = 3$ meters.

Fig. 9 demonstrates the average capacity versus different inter-user distance separating the two ground users. It is observed that the capacity decreases as the inter-user distance increases because increasing the inter-user distance not only increases the propagation distance (resulting in energy loss in free space), but also increases the chance of blockage, and therefore, the UAV needs to fly higher to seek a double-LOS opportunity. In addition, the performance gap between Algorithm 1 and the exhaustive 3D search scheme becomes smaller under larger inter-user distance. In particular, Algorithm 1 achieves about 73% to the exhaustive 3D scheme under the average inter-user distance of 105 meters and about 77% under the average inter-user distance of 175 meters in Map D. Algorithm 2 with $\delta = 3$ meters achieves above 97% to the exhaustive 3D scheme under all inter-user distances both in Map B and Map D.

Fig. 10 evaluates the performance-complexity trade-off of Algorithm 2 in terms of the per-

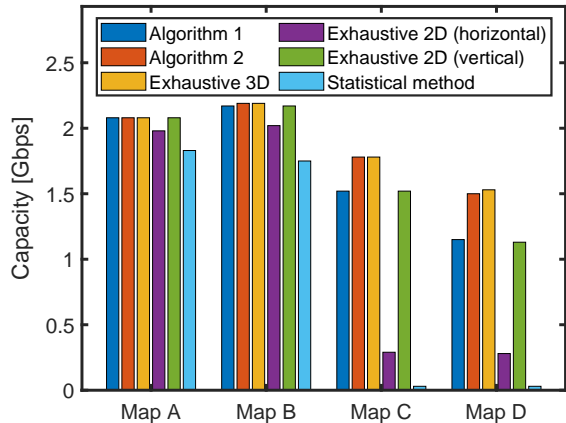


Figure 7. Capacity in different function areas

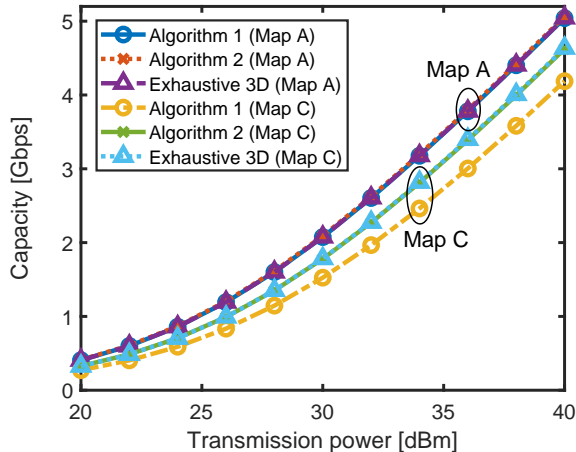


Figure 8. Capacity under different transmission power

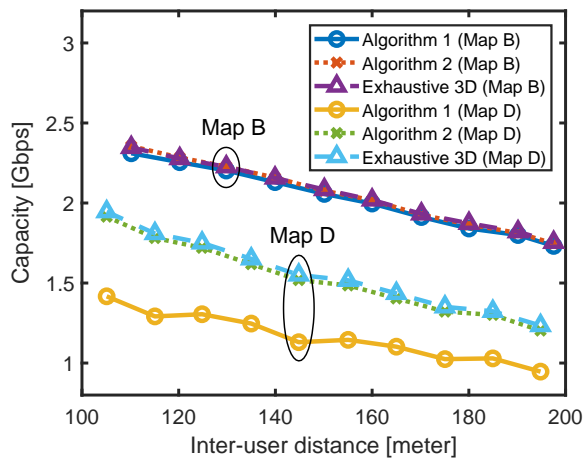


Figure 9. Capacity under different inter-user distance

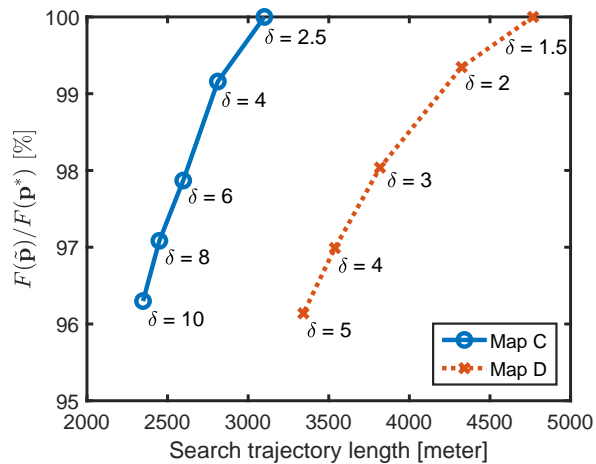


Figure 10. Trade-off of trajectory length and optimality for Algorithm 2

centage of the performance $F(\mathbf{p}^*)$ obtained from the Exhaustive 3D scheme, *i.e.*, $F(\tilde{\mathbf{p}})/F(\mathbf{p}^*)$, over Maps C and D, under transmission power $P = 30$ dBm and $M = 4$. With a choice of $\delta = 4$ meters, Algorithm 2 achieves above 99.1% to the Exhaustive 3D scheme in Map C within 2900-meter search. Additionally, it achieves above 99.3% to the Exhaustive 3D scheme within 4400-meter search in Map D if δ is chosen as 2 meters.

Finally, Table II summarizes the mean trajectory length of different schemes on the four maps. The search lengths of Algorithm 1 and Algorithm 2 with $\delta = 3$ meters are merely several

Table II
COMPARISON OF MEAN TRAJECTORY LENGTH [KILOMETER] UNDER FIVE SCHEMES

Scheme	Map A	Map B	Map C	Map D
Algorithm 1	0.097	0.173	1.715	2.124
Algorithm 2	0.272	0.569	3.002	3.818
Exhaustive 2D (horizontal)	9.353	11.3	185.5	191.5
Exhaustive 2D (vertical)	6.82	7.875	107	110
Exhaustive 3D	546	779.3	21,630	22,590

hundreds of meters for Maps A and B, but both of the algorithms achieve above 99% of the Exhaustive 3D search scheme as seen from Fig. 7. The search lengths of Algorithm 2 are about 3-4 kilometers on Maps C and D to achieve above 98% performance of the Exhaustive 3D scheme (see Fig. 10). This corresponds to 3-4 minutes flight time for a light-weight commercial drone at a cruise speed of 20 m/s.

C. Application in WPT

Fig. 11 shows the average harvested power by the two ground users in the UAV WPT application under transmission power $P = 40$ dBm. First, the relative performance of Algorithm 1 to the global optimality (represented by that of the Exhaustive 3D scheme) decreases as compared to the UAV relay communication as shown in Fig. 7. For example, Algorithm 1 achieves about 80.2% to the Exhaustive 3D scheme over Map C in the WPT application, but it achieves above 85.3% optimality in the relay communication application in Fig. 7. This is because WPT is more sensitive to the propagation distance as observed from its objective function $f(d)$ defined in Section V-A. However, Algorithm 2 with $\delta = 3$ meters still achieves above 98.9% to the Exhaustive 3D scheme over all maps. Second, the performance gain of Algorithm 2 over Algorithm 1 is larger in the WPT application. For example, Algorithm 1 achieves about 76.7% of Algorithm 2 in Map D in the relaying application while it achieves only 66.1% of Algorithm 2 in WPT. Third, the Exhaustive 2D scheme shows poor performance in dense areas (Maps C and D) while it achieves over 90.3% to the Exhaustive 3D scheme in relatively sparse areas (Maps A and B). This is because more blockage leads to fewer chances of finding a double-LOS position close to both users on a fixed horizontal plane, and the power acquisition efficiency decreases

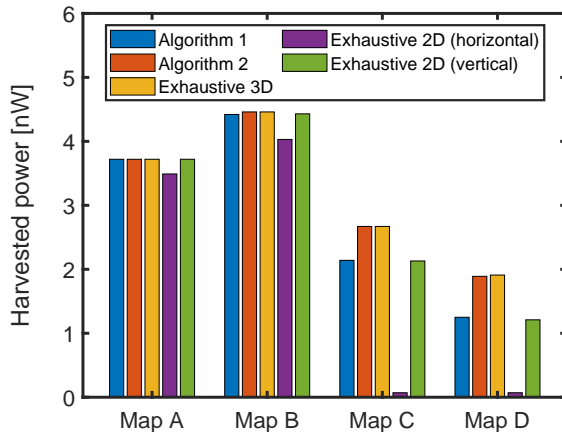


Figure 11. Harvested power in a WPT application

sharply with increasing distance when the UAV flies away from the midpoint of the two users.

VI. CONCLUSIONS

This paper developed two online search algorithms to search for the globally optimal UAV position for establishing LOS links with two ground terminals in deep shadow. A key challenge addressed here was to ensure LOS conditions without the assistance of 3D maps. Exploiting the universal properties of any LOS patterns over an almost arbitrary terrain structure, Algorithm 1 found the optimal position on the middle perpendicular plane with the search length bounded by a linear function of the altitude of the initial point. Algorithm 2 was proposed to search on a bounded 2D local area for the ϵ -optimal UAV position in 3D with search complexity $O(1/\epsilon)$ under some mild condition. The optimality and complexity were further confirmed by numerical experiments with real map data. Both proposed algorithms achieved near 100% global optimality over several real city environments. Additionally, Algorithm 2 achieves above 98.9% performance of the Exhaustive 3D scheme over two simulated dense environments in a WPT application.

APPENDIX A

PROOF OF THEOREM 1

Suppose that the double-LOS trajectory $\hat{\mathbf{p}}(t)$ does not terminate at the globally optimal solution $\hat{\mathbf{p}}$ of \mathcal{P}' . Contradiction can be shown in the following case-by-case discussion.

Case 1: $\hat{\mathbf{p}}(t)$ passes by $\hat{\mathbf{p}}$ at time t_1 , but does not terminate at $\hat{\mathbf{p}}$. Since $\hat{\mathbf{p}}(t)$ only updates when meeting an double-LOS position and each update of $\hat{\mathbf{p}}(t)$ leads to a smaller radius to \mathbf{o} , there exists another double-LOS position $\hat{\mathbf{p}}(t_2)$ such that $F(\hat{\mathbf{p}}(t_2)) > F(\hat{\mathbf{p}}(t_1)) = F(\hat{\mathbf{p}})$, and $t_2 > t_1$. This is a contradiction to the fact that $\hat{\mathbf{p}}$ is the globally optimal solution.

Case 2: $\hat{\mathbf{p}}(t)$ does not pass by $\hat{\mathbf{p}}$. Suppose $\hat{\mathbf{p}}(t)$ terminates at $\hat{\mathbf{p}}(T_1)$ and $\hat{\mathbf{p}}(T_2)$ at the clockwise search stage and the anticlockwise search stage, respectively. Since $\hat{\mathbf{p}}$ is the globally optimal solution of \mathcal{P}' , $F(\hat{\mathbf{p}}(T_1)) \leq F(\hat{\mathbf{p}})$ and $F(\hat{\mathbf{p}}(T_2)) \leq F(\hat{\mathbf{p}})$ result in $r(\hat{\mathbf{p}}(T_1)) \geq r(\hat{\mathbf{p}})$ and $r(\hat{\mathbf{p}}(T_2)) \geq r(\hat{\mathbf{p}})$ according to Lemma 2. Thus, $\hat{\mathbf{p}}$ is embraced by the search trajectory, which implies that the search trajectory $\mathbf{p}(t)$ must pass a point \mathbf{p}' that is perpendicularly above $\hat{\mathbf{p}}$. As Lemma 1 shows that any position perpendicularly above $\hat{\mathbf{p}}$ is also double-LOS, then, the line segment joining $\hat{\mathbf{p}}$ and \mathbf{p}' must be double-LOS. However, according to Step 2a of Algorithm 1, the UAV must go downwards until reaching $\hat{\mathbf{p}}$, leading to a contradiction for Case 2.

To summarize, the double-LOS trajectory $\hat{\mathbf{p}}(t)$ must terminate at the globally optimal solution to \mathcal{P}' .

APPENDIX B

PROOF OF PROPOSITION 2

Denote the plane perpendicular to the ground and passing through points \mathbf{u}_i and \mathbf{a}_i as π_i , $i \in \{1, 2\}$. Define the intersection line of π_1 and π_2 as l_{12} . Given $a_{11}a_{21} > 0$, define a position $\tilde{\mathbf{a}}_i$ on l_{12} such that \mathbf{u}_i , \mathbf{a}_i , and $\tilde{\mathbf{a}}_i$ are colinear and $\tilde{a}_{i3} > 0$. The colinear invariant property of the LOS regions implies that $\tilde{\mathbf{a}}_i$ is LOS from user i , *i.e.*, $\tilde{\mathbf{a}}_i \in \mathcal{D}_0^{(i)}$, given $\mathbf{a}_i \in \mathcal{D}_0^{(i)}$. Then, by applying the upward invariant property of the LOS regions, one can obtain $\tilde{\mathbf{a}}_1$ is a double-LOS position if $\tilde{\mathbf{a}}_1$ is higher than $\tilde{\mathbf{a}}_2$, *i.e.*, $a_{13}/a_{23} > a_{11}/a_{21}$. Otherwise, $\tilde{\mathbf{a}}_2$ is a double-LOS position.

The global optimality can be proved by contradictions. Suppose there exists another double-LOS point $\tilde{\mathbf{a}}$ off l_{12} or there exists another double-LOS point $\tilde{\mathbf{a}}$ lower than both $\tilde{\mathbf{a}}_1$ and $\tilde{\mathbf{a}}_2$ on l_{12} . If so, the intersection point between the middle perpendicular plane and the line joining \mathbf{u}_i and $\tilde{\mathbf{a}}$ will be off the double-ray LOS pattern. This is a contradiction to the unique existence of double-ray LOS pattern. Thus, either $\tilde{\mathbf{a}}_1$ or $\tilde{\mathbf{a}}_2$ is the globally optimal solution to \mathcal{P} since one of them is the lowest double-LOS point on l_{12} .

By applying the knowledge of analytic geometry, one can obtain $\tilde{\mathbf{a}}_1$ and $\tilde{\mathbf{a}}_2$ as

$$\tilde{\mathbf{a}}_1 = \frac{2a_{21}}{a_{11} + a_{21}}\mathbf{a}_1 - \frac{L}{2}\mathbf{e}_2, \text{ and } \tilde{\mathbf{a}}_2 = \frac{2a_{11}}{a_{11} + a_{21}}\mathbf{a}_2 + \frac{L(a_{21} - 2a_{11})}{2a_{11}}\mathbf{e}_2,$$

respectively, where $\mathbf{e}_2 = (\mathbf{u}_2 - \mathbf{u}_1)/\|\mathbf{u}_2 - \mathbf{u}_1\|_2$, and $L = \|\mathbf{u}_2 - \mathbf{u}_1\|_2$.

APPENDIX C

THE CLOSED-FORM SOLUTION TO \mathcal{P}''

Without loss of generality, one only needs to consider the case $b_{21} \geq a_{21} > b_{11} \geq a_{11} > 0$ due to the symmetric properties, and this case offers $\max\{d_1(\mathbf{p}), d_2(\mathbf{p})\} = d_1(\mathbf{p})$. Since $F(\mathbf{p})$ is decreasing with $\max\{d_1(\mathbf{p}), d_2(\mathbf{p})\}$, maximizing $F(\mathbf{p})$ will be equivalent to minimizing $d_1(\mathbf{p})$. According to Proposition 2, if $x_{13}/x_{23} \geq x_{11}/x_{21}$, $\mathbf{q}_1(\mathbf{x}_1, \mathbf{x}_2) = 2x_{21}/(x_{11} + x_{21})\mathbf{x}_1 - L/2\mathbf{e}_2$ will be the 3D globally optimal solution to \mathcal{P} given the LOS pair $(\mathbf{x}_1, \mathbf{x}_2)$ for a double-ray pattern. Otherwise, $\mathbf{q}_2(\mathbf{x}_1, \mathbf{x}_2) = 2x_{11}/(x_{11} + x_{21})\mathbf{x}_2 + L(x_{21} - 2x_{11})/(2x_{11})\mathbf{e}_2$ will be the solution. Here, we consider the case $x_{13}/x_{23} \geq x_{11}/x_{21}$, and the other case is similar to it. Given the above conditions, \mathcal{P}'' can be transformed as the following problem.

$$\begin{aligned}
& \underset{\mathbf{q}_1(\mathbf{x}_1, \mathbf{x}_2)}{\text{minimize}} && d_1(\mathbf{q}_1(\mathbf{x}_1, \mathbf{x}_2)) \\
& \text{subject to} && a_{i1} \leq x_{i1} \leq b_{i1} \\
& && x_{11} \leq x_{21}x_{13}/x_{23} \\
& && \mathbf{x}_1 = (x_{11}, a_{12}, h_1), \mathbf{x}_2 = (x_{21}, a_{22}, h_2).
\end{aligned} \tag{13}$$

The objective function in (13) is decreasing with x_{21} , and it has only one stationary point with x_{11} . In addition, the feasible domains of x_{11} and x_{21} in (13) are bounded while other variables are constants. Then the solving process can be summarized as the following four steps.

- 1) Pick the optimal value $x_{21}^*(x_{11})$ from $x_{21} \in [\max\{a_{21}, x_{11}h_2/h_1\}, b_{21}]$ through the monotonicity of $d_1(\mathbf{q}_1(\mathbf{x}_1, \mathbf{x}_2))$.
- 2) Given $x_{21}^*(x_{11})$, calculate the stationary point of $d_1(\mathbf{q}_1(\mathbf{x}_1, \mathbf{x}_2))$ over x_{11} , and obtain the optimal value x_{11}^* from $x_{11} \in [a_{11}, \min\{b_{11}, x_{21}^*(x_{11}) \cdot h_1/h_2\}]$.
- 3) Calculate the optimal value of x_{21} as $x_{21}^* = x_{21}^*(x_{11}^*)$.
- 4) The solution $\mathbf{q}_1(\mathbf{x}_1^*, \mathbf{x}_2^*)$ can be obtained by substituting $\mathbf{x}_1^* = x_{11}^*\mathbf{e}_1 + a_{12}\mathbf{e}_2 + h_1\mathbf{e}_3$ and $\mathbf{x}_2^* = x_{21}^*\mathbf{e}_1 + a_{22}\mathbf{e}_2 + h_2\mathbf{e}_3$ into formula (5).

The similar method can be applied to other cases. Finally, the solution to \mathcal{P}'' is given as

$$Q(\mathbf{a}_1, \mathbf{b}_1; \mathbf{a}_2, \mathbf{b}_2) = \begin{cases} q_1(\rho_1) & \text{if } |b_{21}| \geq |a_{21}| > |b_{11}| \geq |a_{11}| \text{ and } \frac{h_2}{h_1} \leq \frac{b_{21}}{a_{11}} \\ q_2(\rho_2) & \text{if } |b_{21}| \geq |a_{21}| > |b_{11}| \geq |a_{11}| \text{ and } \frac{h_2}{h_1} > \frac{b_{21}}{a_{11}} \\ q_2(\rho_3) & \text{if } |b_{11}| \geq |a_{11}| > |b_{21}| \geq |a_{21}| \text{ and } \frac{h_2}{h_1} \geq \frac{a_{11}}{b_{21}} \\ q_1(\rho_4) & \text{if } |b_{11}| \geq |a_{11}| > |b_{21}| \geq |a_{21}| \text{ and } \frac{h_2}{h_1} < \frac{a_{11}}{b_{21}} \end{cases} \tag{14}$$

where

$$\begin{aligned}\mathbf{q}_1(\rho) &= \frac{2a_{11}\rho}{\rho+h_1}\mathbf{e}_1 + \frac{(\rho-h_1)L}{2(\rho+h_1)}\mathbf{e}_2 + \frac{2h_1\rho}{\rho+h_1}\mathbf{e}_3, \quad \mathbf{q}_2(\rho) = \frac{2a_{21}\rho}{\rho+h_2}\mathbf{e}_1 + \frac{(h_2-\rho)L}{2(\rho+h_2)}\mathbf{e}_2 + \frac{2h_2\rho}{\rho+h_2}\mathbf{e}_3, \\ \rho_1 &= \max\left\{h_2, \frac{a_{21}h_1}{a_{11}}\right\}, \quad \rho_2 = \text{median}\left\{\frac{a_{11}h_2}{a_{21}}, \frac{b_{11}h_2}{a_{21}}, h_1, h_2, \frac{L^2h_2}{4a_{21}^2+4h_2^2}\right\}, \\ \rho_3 &= \max\left\{h_1, \frac{a_{11}h_2}{a_{21}}\right\}, \quad \rho_4 = \text{median}\left\{\frac{a_{21}h_1}{a_{11}}, \frac{b_{21}h_1}{a_{11}}, h_1, h_2, \frac{L^2h_1}{4a_{11}^2+4h_1^2}\right\}.\end{aligned}$$

APPENDIX D

PROOF OF LEMMA 3

First, it can be easily verified that $\mathcal{B}(\mathbf{p}_0) \subseteq \tilde{\mathcal{B}}(\mathbf{p}_0)$. It follows that, given a double-LOS point \mathbf{p}_0 , the optimal solution \mathbf{p}^* to \mathcal{P} must lie in $\tilde{\mathcal{B}}(\mathbf{p}_0)$ due to the fact that the objective function is decreasing in $d_0(\mathbf{p})$.

Then, for each user $i \in \{1, 2\}$, find the points $\mathbf{p}_i \in \mathcal{S}$ and $\mathbf{p}'_i \in \mathcal{H}$, such that the points \mathbf{u}_i , \mathbf{p}^* , \mathbf{p}_i , and \mathbf{p}'_i are colinear as illustrated in Fig. 3. It is clear that either \mathbf{p}_i or \mathbf{p}'_i belongs to $\tilde{\mathcal{B}}(\mathbf{p}_0) \cap \{\mathcal{S} \cup \mathcal{H}\}$. Specifically, for $d_0(\mathbf{p}_0) \leq \sqrt{2}L/2$, we have $\mathbf{p}_i \in \mathcal{B}(\mathbf{p}_0) \cap \mathcal{S}$ or $\mathbf{p}'_i \in \mathcal{B}(\mathbf{p}_0) \cap \mathcal{H}$; for $d_0(\mathbf{p}_0) \geq L$, we have $\mathbf{p}'_i \in \mathcal{B}(\mathbf{p}_0) \cap \mathcal{H}$; and for $\sqrt{2}L/2 < d_0(\mathbf{p}_0) < L$, we have $\mathbf{p}_i \in \tilde{\mathcal{B}}(\mathbf{p}_0) \cap \mathcal{S}$ or $\mathbf{p}'_i \in \tilde{\mathcal{B}}(\mathbf{p}_0) \cap \mathcal{H}$.

Due to the colinear invariant property for the LOS regions, it suffices to search either \mathbf{p}_i or \mathbf{p}'_i for the LOS status to user i , where both \mathbf{p}_i and \mathbf{p}'_i have the same LOS status.

As a result, given the LOS status found for \mathbf{p}_1 and \mathbf{p}_2 , Proposition 2 asserts that the optimal solution can be found as $\mathbf{p}^* = \mathbf{q}(\mathbf{p}_1, \mathbf{p}_2)$ in (5). Since either \mathbf{p}_i or \mathbf{p}'_i belongs to $\tilde{\mathcal{B}}(\mathbf{p}_0) \cap \{\mathcal{S} \cup \mathcal{H}\}$ and the two points are related according to (7) and (8), it thus suffices to search $\tilde{\mathcal{B}}(\mathbf{p}_0) \cap \{\mathcal{S} \cup \mathcal{H}\}$ for computing \mathbf{p}^* . The result of Lemma 3 is thus proven.

APPENDIX E

PROOF OF THEOREM 2

Consider the region $\mathcal{B}'(\tilde{\mathbf{p}}) \triangleq \{\mathbf{p} \in \mathbb{R}^3 : p_3 \geq H'_{\min}(\tilde{\mathbf{p}}), d_0(\mathbf{p}) \leq d_0(\tilde{\mathbf{p}})\}$. Since $\tilde{\mathbf{p}}$ as the solution to problem (9) is a double-LOS point and $H'_{\min}(\tilde{\mathbf{p}}) < H_{\min}$, we must have $\mathbf{p}^* \in \mathcal{B}'(\tilde{\mathbf{p}})$. In addition, $\mathcal{B}'(\tilde{\mathbf{p}}) \subseteq \mathcal{B}'(\mathbf{p}_0)$. Without loss of generality, consider the case $d_0(\mathbf{p}^*) = d_1(\mathbf{p}^*) > d_2(\mathbf{p}^*)$ which means that \mathbf{p}^* is closer to \mathbf{u}_2 as shown in Fig. 12.

First, given $d_0(\tilde{\mathbf{p}}) \leq \sqrt{2}L/2$, it holds from the geometry that the colinear point \mathbf{p}_1 , w.r.t. \mathbf{u}_1 and \mathbf{p}^* , lies in the effective search region $\mathcal{B}'(\mathbf{p}_0) \cap \mathcal{S}$. Then, define $\bar{\mathbf{p}}_1 \in \mathcal{T}$ as a point

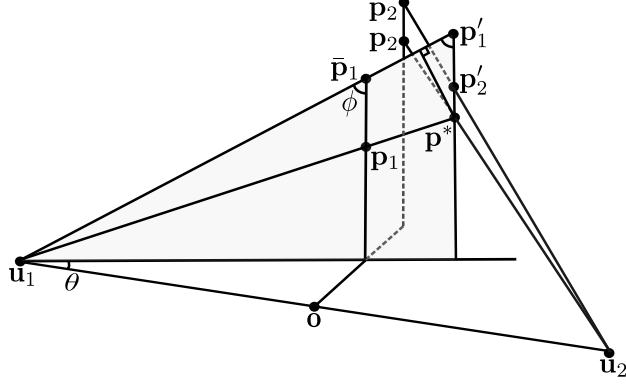


Figure 12. Performance gap due to the vertical step size δ .

on trajectories such that $\bar{\mathbf{p}}_1$ is perpendicularly above \mathbf{p}_1 and the closest to \mathbf{p}_1 . It is clear that $\|\bar{\mathbf{p}}_1 - \mathbf{p}_1\|_2 \leq \delta$, since the trajectories are parallel to the ground with δ space. Additionally, $\bar{\mathbf{p}}_1$ is LOS to \mathbf{u}_1 due to the upward invariant property. Similarly, one can define \mathbf{p}_2 and $\bar{\mathbf{p}}_2$.

Next, define \mathbf{p}'_1 as a point perpendicularly above \mathbf{p}^* such that \mathbf{u}_1 , $\bar{\mathbf{p}}_1$, and \mathbf{p}'_1 are colinear. Similarly, one can obtain the colinear point \mathbf{p}'_2 . Given the LOS status of $\bar{\mathbf{p}}_1$ and $\bar{\mathbf{p}}_2$, Proposition 2 asserts that either $\mathbf{p}'_1 = \mathbf{q}(\bar{\mathbf{p}}_1, \bar{\mathbf{p}}_2)$ or $\mathbf{p}'_2 = \mathbf{q}(\bar{\mathbf{p}}_1, \bar{\mathbf{p}}_2)$ is a double-LOS point, and the other one is a non-double-LOS point. Since $\mathbf{q}(\bar{\mathbf{p}}_1, \bar{\mathbf{p}}_2)$ is a suboptimal solution to problem (9), the double-LOS point \mathbf{p}'_1 or \mathbf{p}'_2 must lie in the feasible set of problem (9). As $\tilde{\mathbf{p}}$ is the solution to problem (9), it holds that $d_0(\mathbf{p}'_1) \geq d_0(\tilde{\mathbf{p}})$ if \mathbf{p}'_1 is double-LOS, and $d_0(\mathbf{p}'_2) \geq d_0(\tilde{\mathbf{p}})$, otherwise.

Without loss of generality, consider \mathbf{p}'_1 is double-LOS. Then, there exists a point $\tilde{\mathbf{p}}'$ perpendicularly above \mathbf{p}^* and below \mathbf{p}'_1 such that $d_0(\mathbf{p}'_1) \geq d_0(\tilde{\mathbf{p}}') = d_0(\tilde{\mathbf{p}}) \geq d_0(\mathbf{p}^*)$. Define ϕ as the angle between $\mathbf{u}_1 - \mathbf{p}'_1$ and $\mathbf{p}^* - \mathbf{p}'_1$, and define θ as the angle between the basis vector \mathbf{e}_2 and the plane containing \mathbf{u}_1 , \mathbf{p}_1 , and $\bar{\mathbf{p}}_1$. Based on the geometric properties, one can obtain

$$d_0(\tilde{\mathbf{p}}) - d_0(\mathbf{p}^*) \leq \|\tilde{\mathbf{p}}' - \mathbf{p}^*\|_2 \cos \phi \leq \frac{2}{L} \|\bar{\mathbf{p}}_1 - \mathbf{p}_1\|_2 d_0(\tilde{\mathbf{p}}) \cos \phi \cos \theta \sin \phi.$$

Given $\cos \theta \leq 1$, $\cos \phi \leq 1$ and $p_{13} \geq H'_{\min}(\tilde{\mathbf{p}})$, the upper bound of $\sin \phi$ is given by

$$\sin \phi \leq \frac{L}{2 \cos \theta \sqrt{(L/(2 \cos \theta))^2 + (p_{13} + \|\bar{\mathbf{p}}_1 - \mathbf{p}_1\|_2)^2}} \leq \frac{L}{2 \cos \theta \sqrt{(L/2)^2 + (H'_{\min}(\tilde{\mathbf{p}}))^2}}.$$

Given $\|\bar{\mathbf{p}}_1 - \mathbf{p}_1\|_2 \leq \delta$ and $\cos \phi \leq 1$, the gap $d_0(\tilde{\mathbf{p}}) - d_0(\mathbf{p}^*)$ is upper bounded by

$$d_0(\tilde{\mathbf{p}}) - d_0(\mathbf{p}^*) \leq \frac{2}{L} \|\bar{\mathbf{p}}_1 - \mathbf{p}_1\|_2 d_0(\tilde{\mathbf{p}}) \cos \phi \cos \theta \sin \phi \leq \frac{2}{L} \delta \sqrt{d_0^2(\tilde{\mathbf{p}}) - H_{\min}^2}. \quad (15)$$

Similarly, one can derive the same gap as (15) if \mathbf{p}'_2 is a double-LOS point. Therefore, the distance gap between $d_0(\tilde{\mathbf{p}})$ and $d_0(\mathbf{p}^*)$ is upper bounded by $2\delta \sqrt{d_0^2(\tilde{\mathbf{p}}) - H_{\min}^2}/L$. As $f(d)$ is

decreasing with d , $f'(d) < 0$, and thus, $f'(d_0(\mathbf{p}^*)) < 0$. Then, the first order condition of the convex function $f(d)$ shows that $f(d_0(\tilde{\mathbf{p}})) - f(d_0(\mathbf{p}^*)) \geq 2\delta f'(d_0(\mathbf{p}^*))\sqrt{d_0^2(\tilde{\mathbf{p}}) - H_{\min}^2}/L$.

One can obtain $F(\mathbf{p}) = \min\{f(d_1(\mathbf{p})), f(d_2(\mathbf{p}))\} = f(d_0(\mathbf{p}))$ using the definition of $d_0(\mathbf{p})$ and the monotonicity of $f(d_i(\mathbf{p}))$. Hence, the performance gap can be obtained as

$$F(\mathbf{p}^*) - F(\tilde{\mathbf{p}}) = f(d_0(\mathbf{p}^*)) - f(d_0(\tilde{\mathbf{p}})) \leq -\frac{2}{L}\delta f'(d_0(\mathbf{p}^*))\sqrt{d_0^2(\tilde{\mathbf{p}}) - H_{\min}^2}.$$

REFERENCES

- [1] C. Wang, J. Huang, H. Wang, X. Gao, X. You, and Y. Hao, "6G wireless channel measurements and models: Trends and challenges," *IEEE Veh. Technol. Mag.*, vol. 15, no. 4, pp. 22–32, 2020.
- [2] C. Wang, J. Wang, S. Hu, Z. H. Jiang, J. Tao, and F. Yan, "Key technologies in 6G terahertz wireless communication systems: A survey," *IEEE Veh. Technol. Mag.*, vol. 16, no. 4, pp. 27–37, 2021.
- [3] Y. Zeng, Q. Wu, and R. Zhang, "Accessing from the sky: A tutorial on UAV communications for 5G and beyond," *Proc. IEEE*, vol. 107, no. 12, pp. 2327–2375, 2019.
- [4] G. Geraci, A. Garcia-Rodriguez, M. M. Azari, A. Lozano, M. Mezzavilla, S. Chatzinotas, Y. Chen, S. Rangan, and M. Di Renzo, "What will the future of UAV cellular communications be? a flight from 5G to 6G," *IEEE Commun. Surveys Tuts.*, 2022, to appear.
- [5] X. Zhong, Y. Guo, N. Li, and Y. Chen, "Joint optimization of relay deployment, channel allocation, and relay assignment for UAVs-aided D2D networks," *IEEE/ACM Trans. Netw.*, vol. 28, no. 2, pp. 804–817, 2020.
- [6] T. Ma, H. Zhou, B. Qian, N. Cheng, X. Shen, X. Chen, and B. Bai, "UAV-LEO integrated backbone: A ubiquitous data collection approach for B5G internet of remote things networks," *IEEE J. Sel. Areas Commun.*, vol. 39, no. 11, pp. 3491–3505, 2021.
- [7] M. Samir, S. Sharafeddine, C. M. Assi, T. M. Nguyen, and A. Ghayeb, "UAV trajectory planning for data collection from time-constrained IoT devices," *IEEE Trans. on Wireless Commun.*, vol. 19, no. 1, pp. 34–46, 2020.
- [8] X. Li, H. Yao, J. Wang, X. Xu, C. Jiang, and L. Hanzo, "A near-optimal UAV-aided radio coverage strategy for dense urban areas," *IEEE Trans. Veh. Technol.*, vol. 68, no. 9, pp. 9098–9109, 2019.
- [9] Y. Liu, K. Xiong, Y. Lu, Q. Ni, P. Fan, and K. B. Letaief, "UAV-aided wireless power transfer and data collection in Rician fading," *IEEE J. Sel. Areas Commun.*, vol. 39, no. 10, pp. 3097–3113, 2021.
- [10] Y. Wang, Z. Su, N. Zhang, and R. Li, "Mobile wireless rechargeable UAV networks: Challenges and solutions," *IEEE Commun. Mag.*, vol. 60, no. 3, pp. 33–39, 2022.
- [11] M. A. Kishk, A. Bader, and M.-S. Alouini, "On the 3-D placement of airborne base stations using tethered UAVs," *IEEE Trans. on Commun.*, vol. 68, no. 8, pp. 5202–5215, 2020.
- [12] S. Lim, H. Yu, and H. Lee, "Optimal tethered-UAV deployment in A2G communication networks: Multi-agent Q-learning approach," *IEEE Internet Things J.*, 2022, to appear.
- [13] S. Zhang, W. Liu, and N. Ansari, "On tethered UAV-assisted heterogeneous network," *IEEE Trans. Veh. Technol.*, vol. 71, no. 1, pp. 975–983, 2022.
- [14] F. Jiang and A. L. Swindlehurst, "Optimization of UAV heading for the ground-to-air uplink," *IEEE J. Sel. Areas Commun.*, vol. 30, no. 5, pp. 993–1005, 2012.
- [15] Y. Zeng, R. Zhang, and T. J. Lim, "Throughput maximization for UAV-enabled mobile relaying systems," *IEEE Trans. on Commun.*, vol. 64, no. 12, pp. 4983–4996, 2016.

- [16] J. Lyu, Y. Zeng, and R. Zhang, "UAV-aided offloading for cellular hotspot," *IEEE Trans. on Wireless Commun.*, vol. 17, no. 6, pp. 3988–4001, 2018.
- [17] A. Al-Hourani, S. Kandeepan, and S. Lardner, "Optimal LAP altitude for maximum coverage," *IEEE Wireless Commun. Lett.*, vol. 3, no. 6, pp. 569–572, 2014.
- [18] M. Gapeyenko, D. Moltchanov, S. Andreev, and R. W. Heath, "Line-of-sight probability for mmwave-based UAV communications in 3D urban grid deployments," *IEEE Trans. on Wireless Commun.*, vol. 20, no. 10, pp. 6566–6579, 2021.
- [19] M. K. Samimi, T. S. Rappaport, and G. R. MacCartney, "Probabilistic omnidirectional path loss models for millimeter-wave outdoor communications," *IEEE Wireless Commun. Lett.*, vol. 4, no. 4, pp. 357–360, 2015.
- [20] O. Esrafilian, R. Gangula, and D. Gesbert, "Learning to communicate in UAV-aided wireless networks: Map-based approaches," *IEEE Internet Things J.*, vol. 6, no. 2, pp. 1791–1802, 2019.
- [21] M. Chen, M. Mozaffari, W. Saad, C. Yin, M. Debbah, and C. S. Hong, "Caching in the sky: Proactive deployment of cache-enabled unmanned aerial vehicles for optimized quality-of-experience," *IEEE J. Sel. Areas Commun.*, vol. 35, no. 5, pp. 1046–1061, 2017.
- [22] I. Bor-Yaliniz, S. S. Szyszkowicz, and H. Yanikomeroglu, "Environment-aware drone-base-station placements in modern metropolitans," *IEEE Wireless Commun. Lett.*, vol. 7, no. 3, pp. 372–375, 2018.
- [23] Y. Chen and D. Huang, "Joint trajectory design and BS association for cellular-connected UAV: An imitation-augmented deep reinforcement learning approach," *IEEE Internet Things J.*, vol. 9, no. 4, pp. 2843–2858, 2022.
- [24] S. K. Singh, K. Agrawal, K. Singh, A. Bansal, C. P. Li, and Z. Ding, "On the performance of laser-powered UAV-assisted SWIPT enabled multiuser communication network with hybrid NOMA," *IEEE Trans. on Commun.*, vol. 70, no. 6, pp. 3912–3929, 2022.
- [25] Y. Zeng, X. Xu, S. Jin, and R. Zhang, "Simultaneous navigation and radio mapping for cellular-connected UAV with deep reinforcement learning," *IEEE Trans. on Wireless Commun.*, vol. 20, no. 7, pp. 4205–4220, 2021.
- [26] S. Zhang and R. Zhang, "Radio map-based 3D path planning for cellular-connected UAV," *IEEE Trans. on Wireless Commun.*, vol. 20, no. 3, pp. 1975–1989, 2021.
- [27] Y. Dong, C. He, Z. Wang, and L. Zhang, "Radio map assisted path planning for UAV anti-jamming communications," *IEEE Signal Process. Lett.*, vol. 29, pp. 607–611, 2022.
- [28] M. T. Dabiri and S. M. S. Sadough, "Optimal placement of UAV-assisted free-space optical communication systems with DF relaying," *IEEE Commun. Lett.*, vol. 24, no. 1, pp. 155–158, 2020.
- [29] P. Yi, L. Zhu, L. Zhu, Z. Xiao, Z. Han, and X. Xia, "Joint 3-D positioning and power allocation for UAV relay aided by geographic information," *IEEE Trans. on Wireless Commun.*, 2022, to appear.
- [30] J. Chen, U. Mitra, and D. Gesbert, "3D urban UAV relay placement: Linear complexity algorithm and analysis," *IEEE Trans. on Wireless Commun.*, vol. 20, no. 8, pp. 5243–5257, 2021.
- [31] D. Gonzalez-Aguilera, E. Crespo-Matellan, D. Hernandez-Lopez, and P. Rodriguez-Gonzalvez, "Automated urban analysis based on LiDAR-derived building models," *IEEE Trans. Geosci. Remote Sens.*, vol. 51, no. 3, pp. 1844–1851, 2013.
- [32] L. Xie, X. Cao, J. Xu, and R. Zhang, "UAV-enabled wireless power transfer: A tutorial overview," *IEEE Trans. Green Commun. Netw.*, vol. 5, pp. 2042–2064, 2021.
- [33] J. Lyu, Y. Zeng, R. Zhang, and T. J. Lim, "Placement optimization of UAV-mounted mobile base stations," *IEEE Commun. Lett.*, vol. 21, no. 3, pp. 604–607, 2017.
- [34] P. Kumar, P. Singh, S. Darshi, and S. Shailendra, "Analysis of drone assisted network coded cooperation for next generation wireless network," *IEEE Trans. Mob. Comput.*, vol. 20, no. 1, pp. 93–103, 2021.